SUPPORTING INFORMATION

Highly electrically conducting glass-graphene nanoplatelets hybrid coatings

E. Garcia[a], A. Nistal[a], A. Khalifa[b], Y. Essa[b], F. Martín de la Escalera[b], M.I. Osendi[a], P. Miranzo[a]*

[a]Institute of Ceramics and Glass (ICV-CSIC), Kelsen 5, 28049 Madrid, Spain.

[b]Aernnova Engineering Solutions Ibérica, Av. de Manoteras 20, 28050 Madrid, Spain.

Corresponding Author:

Prof. Pilar Miranzo
Instituto de Cerámica y Vidrio (ICV-CSIC)
Campus de Cantoblanco, Kelsen 5
28049 Madrid, Spain
e-mail: pmiranzo@icv.csic.es

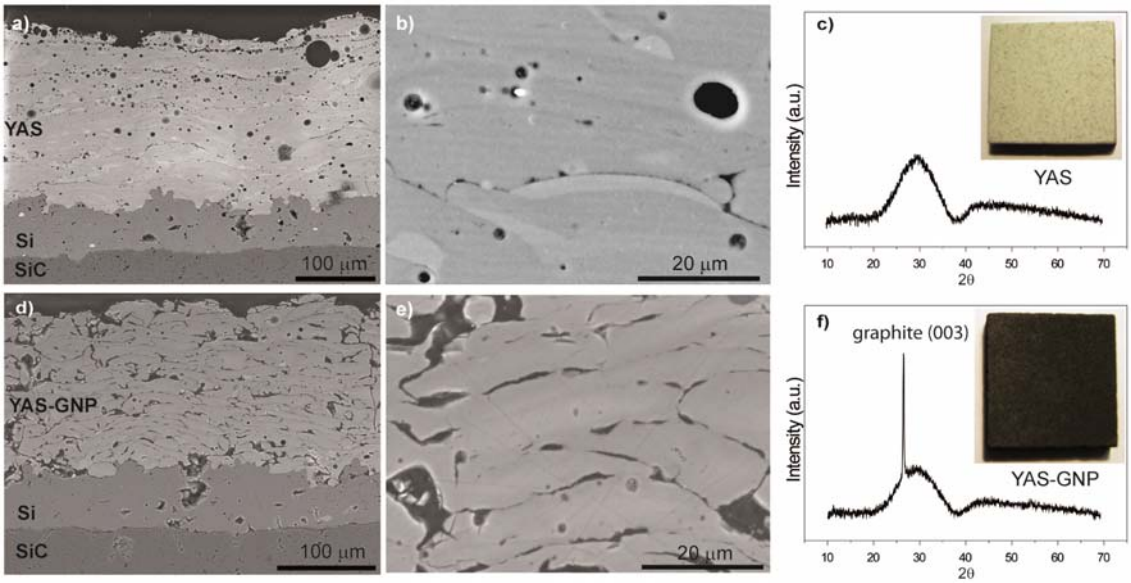

Figure S1. Microstructure and crystalline phase analysis on YAS and YAS-GNP coatings. SEM micrographs of the polished cross-sections of the YAS (a, b) and YAS-GNP (d, e) coatings, showing the common lamellar structure but with evident differences between them. YAS coating contains ~5% (in area) of spherical pores, calculated by image analysis, probably caused by gas entrapment during flame spraying. For the YAS-GNP coating the existence of spherical pores is residual (~1% in area) and nanoplatelets appear situated along the interfaces between lamellas, showing a mostly parallel orientation to the coating surface. The YAS coating appears white to the eye (see optical image in the insert of c) whereas YAS-GNP is black (see insert in f). The corresponding X-ray diffraction patterns of YAS and YAS-GNP coatings shown in (c) and (f) show the amorphous nature of these coatings except for the strong diffraction peak of graphite in the YAS-GNP coating.

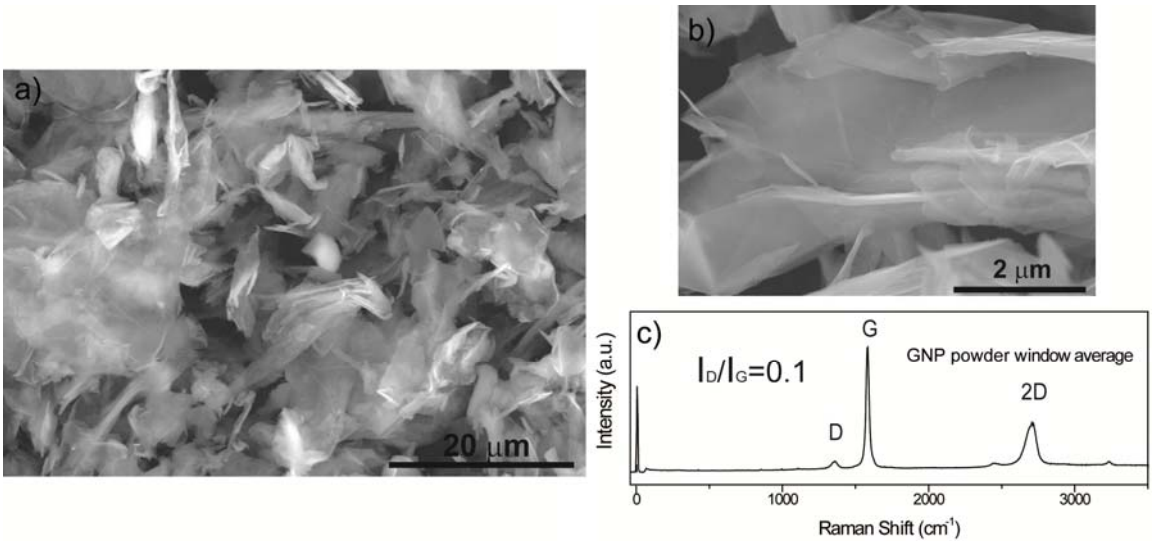

Figure S2. Original GNPs. (a, b) SEM micrographs at two magnifications of the original GNPs. (c) Average Raman spectra of the GNP powder showing the characteristics D, G and 2D bands of graphitic materials; the corresponding I_D/I_G ratio is also shown.

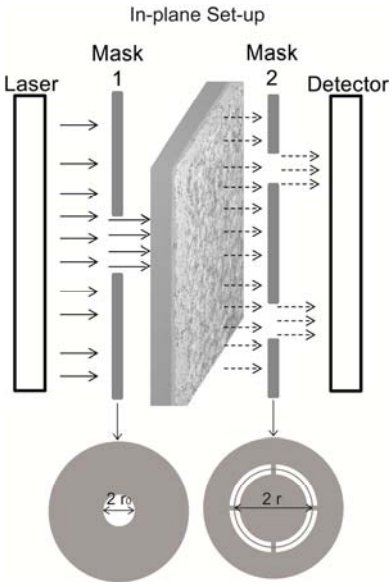

Figure S3. In-plane thermal diffusivity measurement set up. Mask 1 confines the laser pulse into a circle of radius r_0 = 2.5 mm on the center of the sample surface. Accordingly, heat flows through the sample and spreads out on the opposite surface, where a second mask is employed to define an annulus of radius r ($r = 2.2r_0$) facing the IR detector. The temperature rise due to the radial heat flow is fitted by a two-dimensional model that determines an apparent in-plane thermal diffusivity.

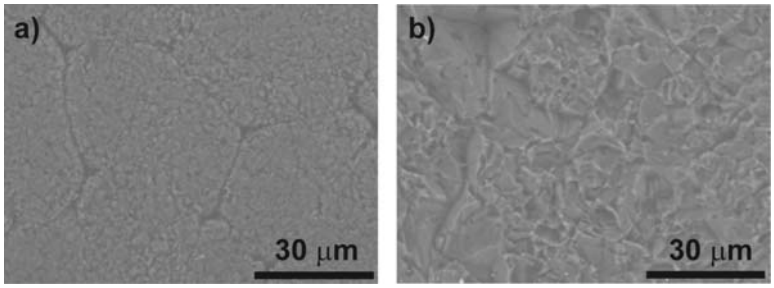

Figure S4. **Surface conditioning of SiC substrates.** SiC plates (Hexoloy® SA, Saint-Gobain, USA) of dimensions 25 × 25 × 4 mm^3 and density of 3.15 $g{\cdot}cm^{-3}$ were used as substrates. The arithmetic average of roughness profile (R_a = 0.24 ± 0.01 µm) of the as-received substrate (a SEM micrograph is shown in a) was not enough for ensuring good mechanical anchoring. Therefore, the substrates were grit blasted with SiC particles of ~0.6 mm of diameter (Navarro SiC, Spain) during 30 s using a pressure of 4 bar and an incident angle of ~45° (Guyson, Formula 1400 UK). The R_a of the SiC grit blasted surface (shown in b) increased up to 3.1 ± 0.2 µm. A Si layer (thickness of ~56 ± 10 µm) was flame sprayed onto the grit blasted SiC plate for better adherence of the coating.

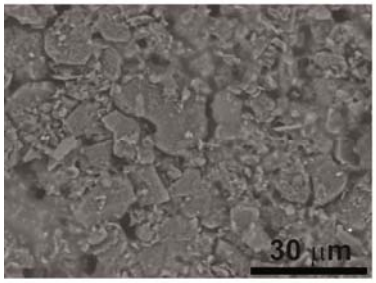

Figure S5: Cordierite substrate. Cordierite substrates (25 × 25 × 5.5 mm^3 plates) were in-house made using cordierite precursor powders (SP-100, VICAR SA, Spain). The raw materials were pressed at 6 MPa and heat treated at 1250 °C for 2 h. The microstructure of the sintered material is shown in the SEM image. Due to the high surface roughness of the cordierite plates (R_a = 9 ± 1 μm), this substrate did not require any surface conditioning prior to the flame spraying process.